Comparative Analysis of Tooth-Root Strength Using ISO and AGMA Standards in Spur and Helical Gears With FEM-based Verification

Andrzej Kawalec
e-mail: ak@prz.edu.pl

Jerzy Wiktor

Rzeszów University of Technology,
Department of Mechanical and Aerospace Engineering,
ul. W. Pola 2,
Rzeszów, PL-35-959,
Poland

Dariusz Ceglarek
Department of Industrial and Systems Engineering,
The University of Wisconsin-Madison,
Madison, WI
e-mail: darek@enger.wisc.edu

Current trends in engineering globalization require researchers to revisit various normalized standards that determine "best practices" in industries. This paper presents comparative analysis of tooth-root strength evaluation methods used within ISO and AGMA standards and verifying them with developed models and simulations using the finite element method (FEM). The presented analysis is conducted for (1) wide range of spur and helical gears manufactured using racks or gear tools; and for (2) various combinations of key geometrical (gear design), manufacturing (racks and gear tools), and performance (load location) parameters. FEM of tooth-root strength is performed for each modeled gear. FEM results are compared with stresses calculated based on the ISO and AGMA standards. The comparative analysis for various combinations of design, manufacturing, and performance parameters are illustrated graphically and discussed briefly. The results will allow for a better understanding of existing limitations in the current standards applied in engineering practice as well as provide a basis for future improvements and/or unifications of gear standards. [DOI: 10.1115/1.2214735]

Keywords: gear design and manufacturing, gear strength, finite element analysis

1 Introduction

1.1 Motivation. Gears are essential to the global economy and are used in nearly all applications where power transfer is required, such as automobiles, industrial equipment, airplanes, helicopters, and marine vessels. Frequency of product model change and the vast amounts of time and cost required to make a changeover, also called time-based competition, has become a characteristic feature of modern global manufacturing and new product development in automotive, aerospace, and other industries [1]. This forces gear manufacturers to respond with improved gear systems that are designed and manufactured faster than before. Simultaneously, current trends in engineering globalization require research to revisit various normalized standards to determine their common fundamentals and those approaches needed to identify "best practices" in industries. This can lead to various benefits including reduction in redundancies, cost containment related to adjustments between manufacturers for missing part interchangeability, and performance due to incompatibility of different standards. Given the range of differences that exist in engineering practices today, frequently manufacturers must seek certificates of their products in Asia, Europe, and/or/ in the USA. This coincides with the recently developed "*Gear Industry Vision in 2025*" strategic goals. The report recommends as one of the five strategic goals to establish common standards with special emphasis on: (i) one global system of design and testing standards by 2015; and (ii) standardized quality and verification procedures [2].

Gear transmissions are widely used in various industries and their efficiency and reliability are critical in the final product performance evaluation. Gear transmissions affect energy consumption during usage, vibrations, noise, and warranty costs among others factors [3–6]. These factors are critical in modern competitive manufacturing, especially in the aviation industry which demands exceptional operational requirements concerning high reliability and strength, low weight and energy consumption, low vibrations and noise. Considering their reliability and efficiency are some of the most important factors, problems of distribution of loads and, consequently, distribution of stresses in the whole gear transmission, particularly in teeth of mating gears, need to be thoroughly analyzed.

Gears have been manufactured for a number of years with extensive ongoing research related to their efficiency, operational quality, and durability. They are relatively complex and there are a number of design parameters involved in gear design. The design of gears requires an iterative approach to optimize design parameters, which govern both the kinematic as well as strength performance. Due to the complex combinations of these parameters, conventional design office practice tends to become complicated and time consuming. It involves selection of appropriate information from a large amount of engineering/standards data available in engineering catalogues and design handbooks. While the knowledge in gearing design is vast, however, there is an acute paucity of research on comparative analysis between various standards and engineering practices. Currently, the most popular standards are ISO and AGMA. These standards vary in selected approaches as well as models and methods resulting in different design solutions obtained for the same gear under the same set of working conditions. Yet, the field lacks systematic comparative analysis of both standards supported and justified by the detailed finite element method (FEM) analysis.

In the ISO standard the finite element method is treated as the most accurate method of gear strength determination (method A) and can be used for verification purposes of the results obtained with other methods. This paper attempts to provide a systematic

Contributed by the Power Transmission and Gearing Committee of ASME for publication in the JOURNAL OF MECHANICAL DESIGN. Manuscript received July 21, 2004; final manuscript received November 18, 2005. Review conducted by Prof. David Dooner.

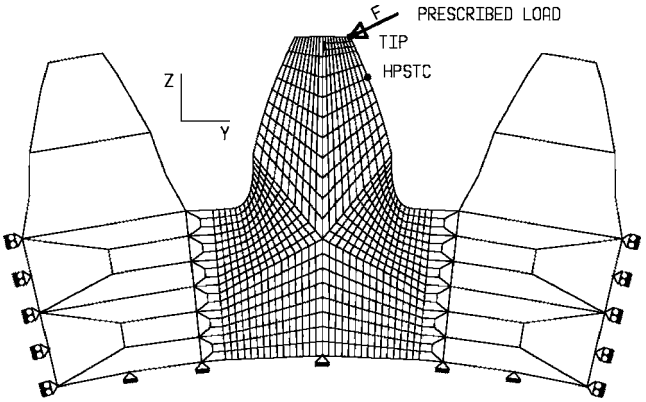

Fig. 1 The finite element model of a segment of a gear and two load cases: prescribed force applied at the tip and prescribed force applied at the highest point of single tooth contact (HPSTC)

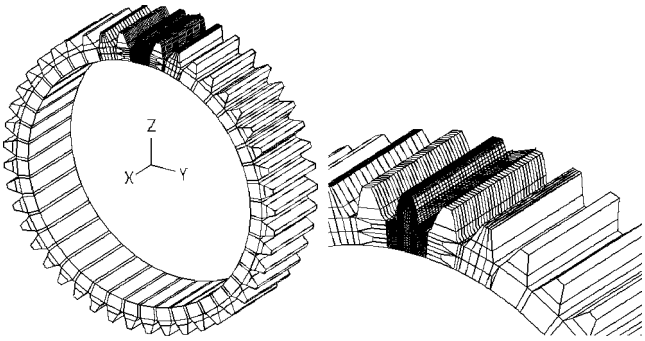

Fig. 3 The FEM model of a representative gear (z=45, m_n =2.75 mm, α_n=20 deg, b=32 mm) made of 3D 20-node isoparametric and eight-node brick finite elements; all degrees of freedom on the internal cylinder of gear disk fixed; load uniformly distributed along the line of contact at the HPSTC; model of the whole gear (left); enlarged view of the loaded tooth (right)

comparative analysis between the ISO and AGMA standards, focused on tooth-root strength, based on the precise FEM modeling of spur and helical gears.

1.2 Literature Review. When the loads occurring in gear transmission cross certain thresholds, very often a fatigue breakage of gear tooth takes place due to repeated high stress exceeding allowable stress limits usually due to improper structure of gear transmission, inappropriate tooth contact, stress concentration around a notch, material defects, and other factors. Tooth breakage results in destroying gear transmission and breaking links between driving and driven shafts. The fracture usually starts at the stretched tooth fillet. Therefore, stress state at tooth root is a representative factor to estimate tooth-root strength of gearings for both involute cylindrical gears with symmetric profiles and for involute spur gears with asymmetric profiles [7] in static and dynamic conditions [8,9].

Accurate evaluation of the stress state and distribution of stresses at tooth root is a complex task. The precise determination of stress distribution requires application of experimental methods using electric resistance wire strain gauges [9,10] or photo-elastic gauges [10,11], digital photoelastic system involving real time imaging [8], as well as numerical methods [4,10,12–15], applying FEM-based simulations [16–18], bipotential equations, and/or utilizing Airy function [11], finite prism method [19], or the theory of Muskhelishvili applied to circular elastic rings [20].

Significant development in analysis of strength properties of gear transmissions follows the achievements in computational design, simulation of meshing, and tooth contact analysis made by Litvin et al. [21,22], Lewicki et al. [23], and Handschuh and Bibel [24]. In particular, Litvin et al. [21] developed an analytical approach for simulation and meshing as well as contact of a face-gear drive with a spur involute pinion, followed by numerical stress analysis of the model of five contacting teeth. In the paper Litvin et al. [22] investigated the contact force and its distribution over contact ellipse, tooth deflection, and load share as well as maximum bending stress along the width of the gear in loaded gear drive. The results of the performed computations were similar to the known experimental ones. Lewicki et al. [23] studied the effect of moving gear load on crack propagation predictions. They performed two-dimensional (2D) analysis using finite element and boundary element methods. Comparison of computed results to experimental ones validated crack simulation based on calculated stress intensity factors and mixed mode crack angle prediction techniques in a model of tooth loaded at the highest point of single tooth contact. Handschuh and Bibel [24] investigated an aerospace-quality spiral bevel gear set numerically and experimentally. The developed nonlinear finite element model allowed

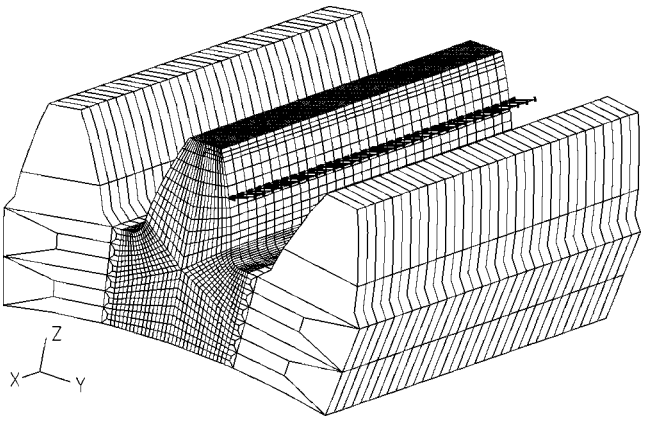

Fig. 2 The FEM model of a representative gear (z=45, m_n =2.75 mm, α_n=20 deg, b=32 mm): segment of three-tooth made of 3D isoparametric 20-node brick finite elements; boundary conditions as in Fig. 1; load uniformly distributed along the line of contact at the HPSTC

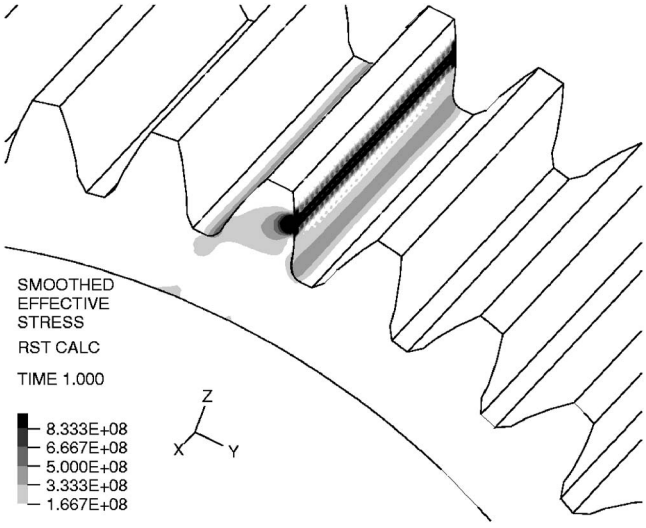

Fig. 4 Distribution of effective stress in the loaded part of the whole gear shown in Fig. 3

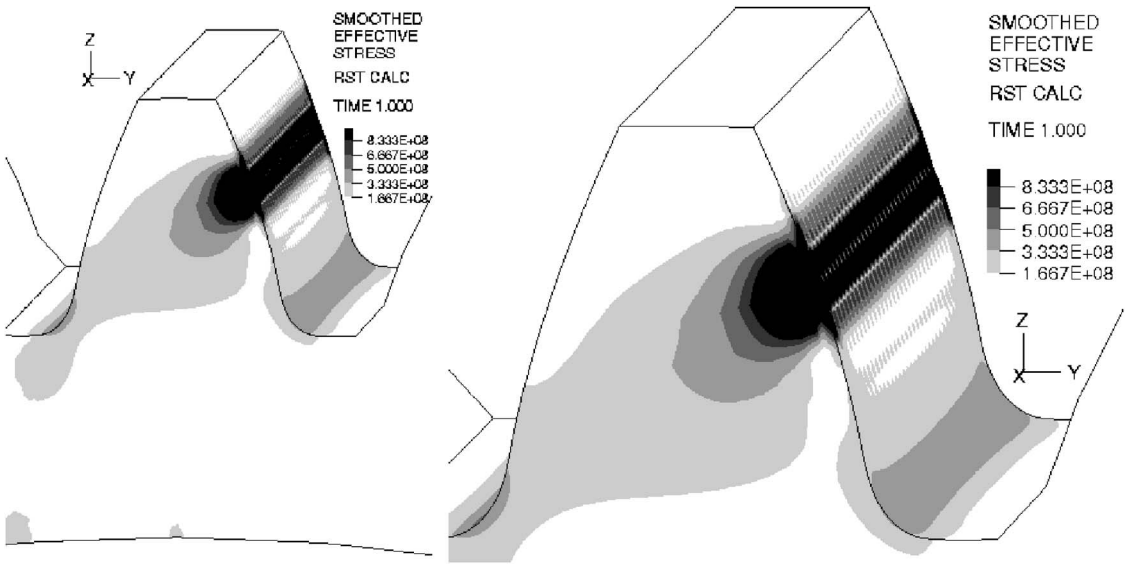

Fig. 5 Distribution of the effective stress in the loaded tooth of the gear shown in Fig. 3

them to simulate three-dimensional (3D) multitooth contact. The results were then compared to experimental ones, obtained with strain gauges. Barkah et al. [25] applied finite element models for static stress evaluation of non-circular gears, focusing on the tooth fillet region. Computed results of stress distributions were in full agreement with existing analytical solutions. Sainsot and Velex [20] developed a new bidimensional analytical model based on Muskhelishvili's theory applied to elastic rings. The model approximates stress distributions at the root circle and allows to calculate gear body-induced tooth deflections more precisely than the Weber's equation, which is based on the semi-infinite plate approximation. Guingand et al. [19] applied the finite prism method (FPM) for quasi-static analysis of helical gears to build a model of cylindrical gears with reduced computational complexity as compared to conventional FEM models. The developed FPM models allow computing load and tooth-root stresses. Velex and Baud [9] experimentally investigated quasi-static and dynamic tooth-root stresses in spur and helical gears and compared them with numerical predictions obtained by using FEM. They developed a specific FE model which accounts for non-linear time-varying mesh stiffness, tooth geometrical errors, and flexural-torsional-axial couplings. However, they did not consider the gear fabrication process, thus their simulations model does not allow to analyze the impact of the fillet shape on tooth-root stresses.

The development in analysis of gear strength shown in papers [21–25] validates the use of correctly defined finite element models for analysis of not only spur or helical gears, but also other types of gears, like hypoid or spiral-bevel gears, etc. Experimental methods, though necessary for validation of theoretical and numerical analyses, are especially complicated, expensive, and laborious. Therefore, they are applied mainly in special cases. In practice, simplified formulas are usually used in gear transmission design. They enable estimation of stresses at tooth root with accuracy acceptable for engineering design.

In every case, strength properties of gear transmissions are strongly influenced by gear geometry, applied manufacturing processes, and dimensional accuracy of manufactured gears [4,12,13,18]. For example, investigations described in Liu and Pines' paper [26] illustrate that some fundamental gear design parameters such as diametral pitch (proportional to the normal module, used in Europe as the characteristic parameter in gear design), pressure angle, and number of teeth, may have a signifi-

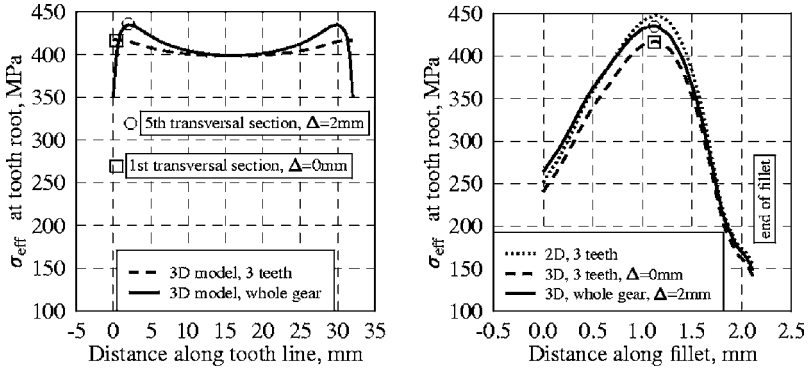

Fig. 6 Comparison of effective stress distributions along tooth line and along fillet of the same gear computed with the use of different finite element models: (i) the whole spur gear built of 3D 20-node isoparametric and eight-node brick finite elements; (ii) segment of three teeth built of 3D 20-node isoparametric brick finite elements; and (iii) segment of three teeth built of eight-node plane stress finite elements; distance Δ describing location of transversal section of tooth is shown in Fig. 7 right

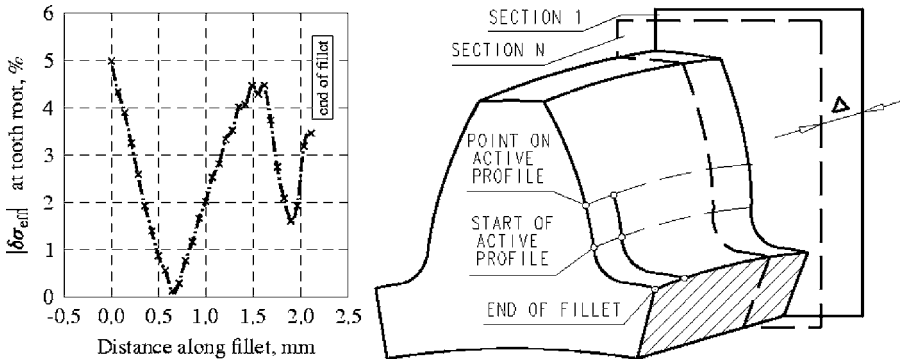

Fig. 7 Absolute values of obtained differences in the effective stresses along fillet $\delta\sigma_{eff}$ computed according to Eq. (1) for the 2D plane stress model with three teeth and for the model of the whole gear built of 3D 20-node isoparametric and eight-node brick finite elements in sections associated with $\Delta=2$ mm (left); explanation of the sections and the lines where the effective stresses are compared (right)

cant influence on damage detection sensitivity. In the aforementioned investigations, the three main types of gear damage were considered: pitting and wear of tooth flanks, concentration of stress, and cracks at tooth root.

The final geometry of every gear depends on the assumed gear structural parameters and the applied manufacturing processes, applied tools, tool machines, etc. [3,12,13,18]. Therefore, the established standards consider models of both gear structures and manufacturing techniques, and take into account certain structural factors, mostly geometric and operational, as well as information concerning applied manufacturing processes, applied tools, and materials. In particular, suitable international ISO [27] standards developed over the years in Europe (or fully compatible German standard DIN [28]), and American standard AGMA [29–37] describe procedures for approximate calculations of stresses at tooth root of the involute gearings. In all these standards evaluation of tooth-root strength is performed based on maximum stress at tooth root on the stretched side of the tooth. Moreover, in all of these standards it is assumed that the maximum stress occurs in the critical section of the tooth. It is clear that proper evaluation of maximum bending stress at tooth root is one of the most critical parameters determining whether or not a particular gear transmission will function properly. Tooth breakage due to operating stress that significantly exceeds the maximum allowable stress in gear transmission can be extremely dangerous in automotive, aerospace, or space industries [3,4,38,39]. Therefore, an accurate estimation of critical strength parameters is of great importance in such cases.

The models considered in ISO and AGMA standards are similar from both theoretical and computational points of view, though they are not identical. They have been developed using state of the art industrial practice as well as theoretical and experimental research in this field. However, there are a number of discrepancies within the current standards. These discrepancies can be classified as: (1) each standard defines different geometrical parameters as critical for gear performance; (2) the calculations undertaken to estimate the thresholds for these critical parameters are based on different assumptions and on different mathematical relations following them; and (3) results of computations differ for each standard under the same conditions.

Currently, there is a need to unify both standards [35]. Initial studies, which intended to compare both standards, were done by Hösel [36,37]. However, Hösel only considered the older versions of the standards, thus limiting his analysis to simple numerical comparison of both standards without any other verification of computed results.

In this paper corresponding models of gears, computational methods used for their analysis, and results obtained according to the ISO and AGMA standards are briefly described and compared with each other. In the next step we verify these with the use of the developed FEM models and simulations. This approach allows

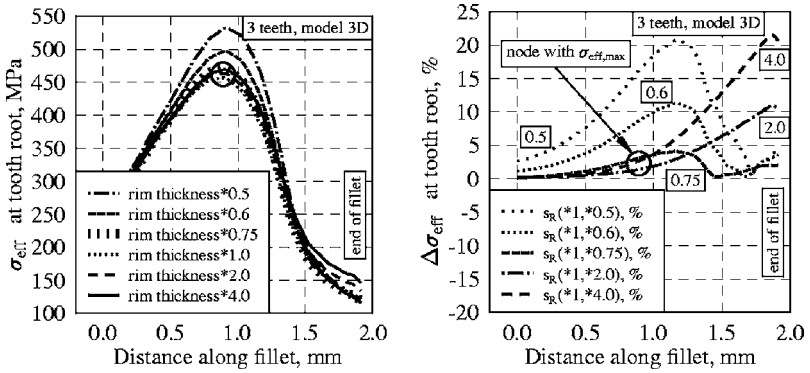

Fig. 8 Comparative analysis of the effective stress distribution at tooth root for three magnitudes of rim thickness of gear (left); absolute values of the relative differences in the effective stresses along fillet $\Delta\sigma_{eff}(^*1, ^*i)$ computed according to Eq. (2) for the model of three-teeth segment of gear built of 3D 20-node isoparametric, for load applied at the HPSTC $F_{bn}/b=500$ N/mm (right)

Table 1 Tooth load

ISO	AGMA
Straight tooth gearings: According to method B (accurate computational method) maximum stress at tooth root is calculated for the load applied at the HPSTC (for gear transmission with the transverse contact ratio $1<\varepsilon_{\alpha n}\leq 2$) or at the highest point of double tooth contact (for $2<\varepsilon_{\alpha n}\leq 3$). According to method C (simplified computational method) maximum stress at the tooth root is calculated for the load applied at the tooth tip. Then, with the use of the coefficient Y_e it is converted to the stress generated with the load applied at the HPSTC [27].	***Straight tooth gearings:*** Maximum stress at tooth root is calculated for transmitted load applied at the HPSTC (the standard allows calculation of stresses for the load applied at the tooth tip) [29].
Helical gearings: Maximum stress at tooth root is calculated for the virtual gearings with straight tooth (with virtual number of teeth z_n) and for load applied at the tip. Transmitted load in the plane of action normal to the tooth flank is converted to the tangential load at the operating pitch diameter [27]: $$F_t=\frac{2000T_{1,2}}{d_{1,2}}$$ where: F_t - tangential load at the operating pitch diameter [N]; $T_{1,2}$ - pinion torque (1), wheel torque (2) [Nm]; $d_{1,2}$ - operating pitch diameter of pinion (1), wheel (2) [mm]. Next, unit tooth load is calculated: $$\frac{F_t}{bm_n}$$ where: b - facewidth [mm]; m_n - normal module [mm].	***Helical gearings:*** Maximum stress at tooth root is calculated for the virtual gearings with straight tooth (with virtual number of teeth z_n) and for the load applied at the tooth tip [29]. Transmitted load in the plane of action normal to the tooth flank is converted to the tangential load at the reference diameter [33] $$F_{wt}=\frac{2000\ T_{1,2}}{d_{w1,2}}$$ where: F_{tw} - tangential load at the reference diameter [N]; $T_{1,2}$ - pinion torque (1), wheel torque (2) [Nm]; $d_{1,2}$ - reference diameter of pinion (1), wheel (2) [mm]. Next, unit tooth load is calculated [33]: $$\frac{F_{wt}}{bm_n}$$ where: b - facewidth [mm]; m_n - normal module [mm].

for better understanding of existing limitations in the current standards as applied in engineering practice and will provide a basis for future improvements of the standards.

1.3 Approach. In both the ISO and AGMA standards, stresses at tooth root are calculated for load applied at the highest point of single tooth contact, i.e., at the HPSTC (in the case of spur gearings) or at the tooth tip (in the case of helical gearings). In the case of helical gears, calculations are performed for the virtual gear with straight teeth and virtual number of teeth denoted z_n. The analysis is conducted in three steps to calculate: (i) transmitted load; (ii) nominal tooth-root stress σ_{FO}; and, (iii) local stress at the tooth root, i.e., to the tooth-root stress σ_F.

Transmitted load in the plane of action, which is normal to the tooth flank, is converted to the nominal tangential load at the reference diameter F_t (according to the ISO standard) or to the transmitted tangential load at the operating pitch diameter F_{wt} (according to the AGMA standard). For a given load, the *nominal tooth-root stress* σ_{FO} is calculated with consideration to the tooth fillet shape and stress concentration caused by the notch. Then, the nominal tooth-root stress is converted using load factors to the *local stress at the tooth root*, i.e., to the tooth-root stress σ_F. The load factors take into account increase of stresses caused by misalignments in manufacturing of gear transmission, external and internal dynamic loads acting on gear transmission, as well as non-uniform distribution of load.

The FEM simulation models of tooth-root strength use a method for computations of tooth profiles as presented in Ref. [40]. This method allows for accurate computation of real tooth profile, including fillet for both tools rack or gear tool. Additionally, the results are automatically interpreted by the software described in Ref. [40]. The development of the precise FEM model of gear tooth requires accurate determination of tooth profile with consideration of the selected machining process of gear fabrication. Such methods are described in Refs. [40,41].

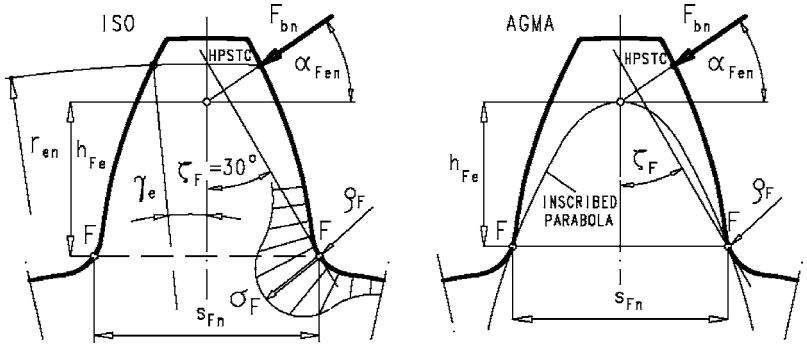

Fig. 9 Determination of the critical section location, angle ζ_F and parameters of the critical section s_{Fn}, h_{Fe}, and ρ_F; according to the ISO and the AGMA standards (for comparison see Table 7 in the Appendix)

Table 2 Methods of determination of the critical section

ISO	AGMA
Based on calculations and analysis of experimental results it is assumed that the critical section is determined by the points of tangency of the fillet with the straight lines inclined at 30 deg to the tooth center line (Fig. 9, left)	Location of the critical section is determined on the basis of the modified Lewis method (Fig. 9, right). The tooth is considered as a beam fixed at its root and loaded with the transmitted load. The critical section is determined by the tangency points of a parabola inscribed into the tooth profile. This parabola represents profile of the beam with uniform strength along its axis.
Therefore, the angle ζ_F between tooth center line and tangent to fillet at the critical point F is constant and independent from shape of the fillet and from location of applied load: $\zeta_F=30$ deg	The angle ζ_F between tooth center line and tangent to fillet at the critical point F is not constant - its value depends on profile of the fillet and on location of the point where load is applied. In the examples considered in this paper the load is applied at the tip and the angle ζ_F which varies (depending on parameters of the gear and machining tool) within the range: $\zeta_F=13-16$ deg. For load applied at the HPSTC the angle ζ_F varies within the range: $\zeta_F=24-30$ deg

It should be noted that the ISO and AGMA standards do not provide procedures for calculation of the whole tooth profile. The standards describe ways to calculate the main parameters of the basic rack profile. In addition, the formulas given in each of the standards do not cover all range of gear manufacturing tools used in industrial practice.

For the sake of comparative analysis the following conditions and assumptions are made:

(1) Loads applied in the FEM, ISO, and AGMA standards are the same.
(2) There are no misalignments in gear transmission, and loads are static and uniformly distributed.
(3) Location of the critical tooth section and maximum tooth-root stresses were calculated following the procedures of the ISO [27] and AGMA [29–35] standards. Both standards provide formulas for calculation of tooth-root stress at the critical section while the conducted FEM simulations allow obtaining the whole distributions of stresses in the modeled gears. From those distributions of stresses the maximum tooth-root stresses with their locations were found by scanning the FEM results.
(4) The notation follows both ISO [27] and AGMA standards [29–35]. Regarding the analysis and computations focused on the ISO procedures, the whole notation is based on the ISO standard [27]. Concerning analysis and computations focused on the ISO procedures in cases where the presented notation is the same for both standards, only the ISO notation is used in order to emphasize similarities between the standards. Other parameters used in formulas are denoted according to the ANSI/AGMA 2101-C95 [33] and AGMA 908-B89 [29] standards. The nomenclature list for both standards is presented in Table 7 in the Appendix.

The details of the related approaches, computational models, methods of calculations, and results are presented in the tables and figures included in the following sections. The outline of the paper is as follows. Section 2 presents the FEM-based approach used for calculation and analysis of gear strength at tooth root. Section 3 describes the loads, critical section definition, and parameters, coefficients, and load factors used in computations as well as recalculations of nominal tooth-root stresses to local tooth root stress. In Sec. 4, tooth-root stress analysis following the ISO, AGMA, and FEM procedures is presented. Finally, the results are summarized and conclusions are drawn in Sec. 5.

2 FEM Modeling

Spur and helical gear models were analyzed based on formulas given in the ISO and AGMA standards as well as based on the

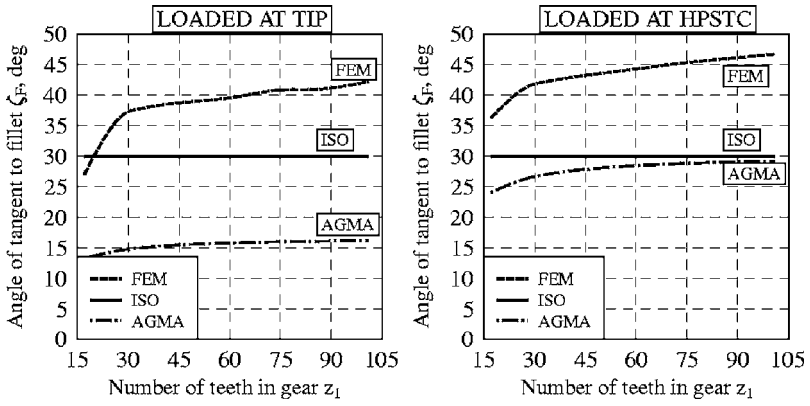

Fig. 10 Influence of the number of gear teeth on the angle ζ_F between tooth centerline and tangent to fillet at the critical point F according to the ISO standard, AGMA standard, and FEM: load applied at the tip (left), load applied at the HPSTC (right); main parameters of the gear: $m_n=2.75$, $\alpha_n=20$ deg, $s_1=4.265$, $\beta_1=0$ deg, main parameters of the rack: $\alpha_0=20$ deg, $s_0=4.320$, $h_{fP}=1.22m_n$, $\rho_{fP}=0.18m_n$

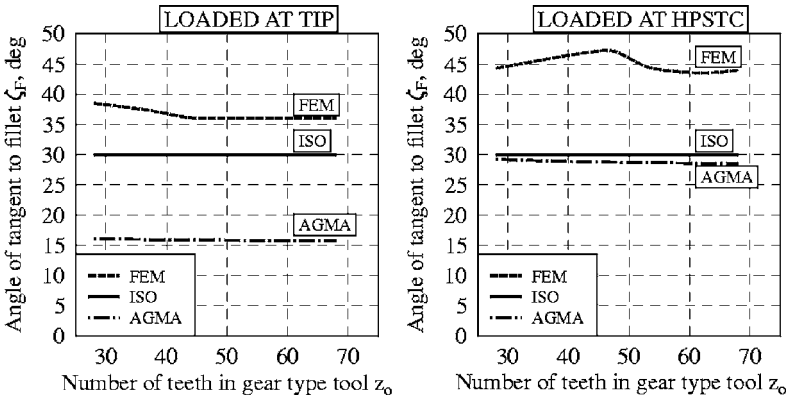

Fig. 11 Influence of the number of teeth z_0 of the gear tool on the angle ζ_F between tooth centerline and tangent to fillet at the critical point *F* according to the ISO standard, AGMA standard, and FEM: load applied at the tip (left), load applied at the HPSTC (right); main parameters of the gear: $m_n=2.75$, $z_1=45$, $\alpha_n=20$ deg, $s_1=4.265$, $\beta_1=0$ deg, main parameters of the gear tool: $\alpha_0=20$ deg, $s_0=4.320$, $h_{fP}=1.22m_n$, $\rho_{fP}=0.18m_n$

conducted FEM modeling [16–18]. FEM computations of stress distribution, as presented in this paper, require precise modeling of tooth, especially accurate representation of its fillet, which constitutes a typical geometric notch. Therefore, a specialized mesh generating program integrated with the ADINA [42] finite element system was developed. The developed program allows for parametric and automatic generation of well shaped finite element meshes for two-dimensional (2D) and three-dimensional (3D) problems with consideration to proper node numbering and required tooth fillet profile [40]. A precise representation of the whole tooth profiles in their various sections was based on cubic Hermite splines and on the least squares approximations [43,44]. The three-dimensional geometric models of tooth profiles were transformed to the ADINA system [42] for further finite element analyses.

Considering the geometric symmetry of the gear only certain gear segments were defined and used for FEM computations. They represented plane stress models made of the eight-node isoparametric plane stress finite elements for spur gears and 3D models made of isoparametric 20-node and eight-node brick finite elements for spur and helical gears. All nodes at the internal circle of gear rim in models considered in this work had all degrees of freedom (DOE) fixed. In addition, the nodes at both radial boundary sections had all DOF fixed, except the ones which are related to radial movements. All nodes at both radial boundary conditions

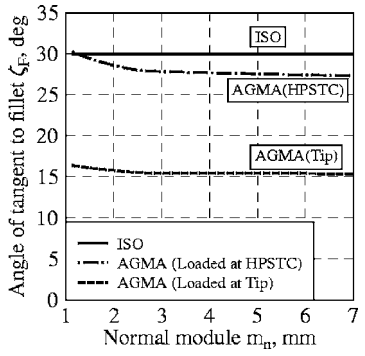

Fig. 12 Influence of the normal module m_n on the angle ζ_F between tooth centerline and tangent to fillet at the critical point *F* according to the ISO standard, AGMA standard for load applied at the tip (Tip), and at the HPSTC; main parameters of the gear: $z_1=45$, $\alpha_n=20$ deg, $\beta_1=0$ deg; main parameters of the rack: $\alpha_0=20$ deg, $h_{fP}=1.25m_n$, $\rho_{fP}=0.5$

were defined in their local coordinate systems (Fig. 1). According to the ISO and AGMA standards the models were loaded at tooth tip or at the highest point of single tooth contact with corresponding prescribed load (Fig. 1). Considering load distribution along the path of contact associated with (i) contact of a single pair of mating teeth, or (ii) simultaneous contact of two pairs of mating teeth, the load applied at tooth tip was half of the load applied at the HPSTC.

The selected plane stress model (Fig. 1) is the most suitable for strength analysis of spur gears presented in this paper. The selection of the plane stress model for strength analysis of spur gears is based on fulfilment of necessary conditions for replacement of 3D strength analysis with plane stress strength analysis of structures [45] like spur gears (much longer face width than whole depth, same shape in each transversal section, uniform load distribution along tooth line) as well as on conducting a large number of two- and three-dimensional finite element gears simulations. The mesh is chosen to satisfy: (i) accuracy requirements for modeling of tooth shape; and (ii) to properly represent necessary boundary conditions, which are located far from the fillets of loaded tooth and region of load application. Following recommendations of Kawalec and Wiktor [44], the optimum mesh density was generated and selected using the criterion of change in the maximum effective stress, i.e., the mesh density in the volume of tooth root is increased until the changes in the maximum effective stress at tooth root $\sigma_{\text{eff,max}}$ are less than 0.4%. In order to compare results of plane stress models with three-dimensional ones several 3D FEM models were developed and analyzed: (1) models built of eight-node 2D isoparametric plane stress elements; (2) models built of 20-node 3D isoparametric brick elements; and (3) models built of 20-node isoparametric and eight-node brick 3D finite elements (FEs). Two of the models are shown in Figs. 2 and 3. Figures 2 and 3 also show the key parameters of gears used in this paper.

The simulations conducted in the paper for 3D models use load, which is uniformly distributed along tooth line and corresponds to the point load applied in plane stress models. The application of load uniformly distributed along tooth line as well as point load is justified, according to the Saint-Venant's principle [45]. That principle states that self-equilibrated systems of tractions result in stresses that decay rapidly with distance from the region where tractions are applied. In other words, in the cases of simulations of bending stresses at tooth root which are considered in this paper, the tooth root is located far from the area of load application, and thus, the overall load forces can be replaced with the equivalent static forces having the same total moments and the same resultant

Table 3 Parameters of the critical section

ISO	AGMA
The ISO standard describes how to calculate the parameters of the critical section for gearings generated with rack. In the case of gearings generated with gear tool (e.g., with gear-shaper cutter) the real tool is in the a.n. procedure of calculations replaced with a virtual one—a rack with the same reference tooth profile. It significantly simplifies calculations, but can lead to erroneous results. The tooth profile generated with the gear tool differs from the one generated with the rack. Therefore, parameters calculated for the virtual rack can significantly differ from the real ones. This may lead to errors in estimation of tooth-root strength, due to wrong results of stress calculations.	The AGMA standard contains procedure of calculation of the parameters of the critical section for gearings generated with gear tool. In the case of gearings generated with rake the calculations are performed the same way, but the rack is represented by the gear tool witha very large number of teeth, i.e. $z_0=10{,}000$. The parameter of the critical section calculated in such a way are comparable with the real ones. The differences can be omitted as far tooth-root strength of gears generated with racks is concerned.
Formulas determining parameters of the critical section are derived from the geometric relations given in Fig. 13 (up) which shows both machined gear and generating rack in a position in which the rack generates point F belonging to the fillet (the point which determines location of the critical section).	Formulas determining parameters of the critical section are derived from the geometric relations given in Fig. 13 (bottom) which shows both machined gear and generating gear tool in a position in which the tool generates point F belonging to the fillet (the point which determines location of the critical section).
Tooth-root chord at the critical section s_{Fn}: $$\frac{s_{Fn}}{m_n}=z_n \sin\left(\frac{\pi}{3}-\vartheta\right)+\sqrt{3}\left(\frac{G}{\cos\vartheta}-\frac{\rho_{fP}}{m_n}\right)$$	Coordinates of the critical point F [29]: $$\xi_{nF}=r_{wn1}\sin\varphi_{n1}+K_F\cos\zeta_F$$ $$\eta_{nF}=r_{wn1}\cos\varphi_{n1}+K_F\sin\zeta_F$$ Tooth-root chord at the critical section s_{Fn}: $s_{Fn}=2\xi_{nF}$
Radius of fillet at the critical section ρ_F: $$\frac{\rho_F}{m_n}=\frac{\rho_{fP}}{m_n}+\frac{2G^2}{\cos\vartheta(z_n\cos^2\vartheta-2G)}$$	Radius of fillet at the section ρ_F: $$\rho_F=\rho_{fP}+\frac{K_S^2}{\frac{r_{wn1}r_{wn0}\cos\vartheta}{r_{wn1}+r_{wn0}}-K_S}$$
Bending moment arm application at the tip h_{Fe}: $$\frac{h_{Fe}}{m_n}=\frac{1}{2}\left[(\cos\gamma_e-\sin\gamma_e tg\alpha_{Fen})\frac{d_{en}}{m_n}\right]-\frac{1}{2}\left[z_n\cos\left(\frac{\pi}{3}-\vartheta\right)+\frac{G}{\cos\vartheta}-\frac{\rho_{fP}}{m_n}\right]$$	Bending moment arm application at the tip h_{Fe} $$h_{Fe}=\frac{r_{bn1}}{\cos\alpha_{Fen}}-\eta_{nF}$$
Analysis of the geometric relations shown in Figs. 9 and 13 leads to the following equation from which an auxiliary angle ϑ can be calculated in an iterative procedure:	where: $$K_S=r_{wn0}\cos\vartheta-r_{Rn0}\cos(\varphi_{Rn0}-\vartheta)$$ $$K_F=K_S-\rho_{fP}$$

forces. The results of FEM stress simulations are shown in Figs. 4–6 and 8. From analysis of tooth stress distribution, the following conclusions can be drawn (see also Figs. 4 and 5): large stresses in the area of load application and at the fillet are separated from each other by the area of very low stresses. Therefore, considering obtained distributions of stresses and the Saint-Venant's principle applied to bending of tooth caused by load transmitted between teeth in mesh, the propagation of errors from point or distributed loadings of tooth to the area/volume at the fillet can be neglected.

Figure 6 contains comparison of distributions of von Mises effective stress along fillet of the same gear computed with the use of different finite element models: (1) the whole gear built of 3D 20-node isoparametric and eight-node brick finite elements; (2) segment of three teeth built of 3D 20-node isoparametric brick finite elements; and (3) segment of three teeth built of eight-node plane stress finite elements.

Relative differences in distributions of the effective stresses along fillet $\boldsymbol{\delta\sigma}_{\text{eff}}$ for the 2D plane stress model with three teeth $\boldsymbol{\sigma}_{\text{eff,(2D)}}$ and for the model of the whole gear built of 3D 20-node isoparametric and eight-node brick finite elements $\boldsymbol{\sigma}_{\text{eff,(3D)}}$ were computed according to the formula:

$$\boldsymbol{\delta\sigma}_{\text{eff}}=\frac{\boldsymbol{\sigma}_{\text{eff,(2D)}}-\boldsymbol{\sigma}_{\text{eff,(3D)}}}{\boldsymbol{\sigma}_{\text{eff,(2D)}}}100 \tag{1}$$

Absolute values of the computed differences $\boldsymbol{\delta\sigma}_{\text{eff}}$ are shown in Fig. 7. From the performed analysis it follows that the maximum difference in tooth-root stresses between the 2D model (Fig. 1) and the 3D model of the whole gear (Fig. 3) are less than 5%.

Strength computations of gears require analysis of the rim thickness [46,47]. Therefore, in order to investigate the influence of rim thickness s_R on the maximum tooth-root strength, various 3D models of three teeth segments of gear with different magnitudes of rim thickness s_R made of the 20-node isoparametric finite elements were computed. Relative differences in distributions of the effective stresses along fillet $\boldsymbol{\Delta\sigma}_{\text{eff}}({}^*1,{}^*i)$ for the 3D models of three-tooth segments of gear with various magnitudes of rim thickness i^*s_R were computed according to the formula:

$$\boldsymbol{\Delta\sigma}_{\text{eff}}({}^*1,{}^*i)=\frac{|\boldsymbol{\sigma}_{\text{eff,max}}({}^*1)-\boldsymbol{\sigma}_{\text{eff,max}}({}^*i)|}{\boldsymbol{\sigma}_{\text{eff,max}}({}^*1)}100 \tag{2}$$

where $i\in\{0.5,0.6,0.75,2.0,4.0\}$, and $\boldsymbol{\sigma}_{\text{eff,max}}({}^*1)$, $\boldsymbol{\sigma}_{\text{eff,max}}({}^*i)$ denote the maximum tooth-root stress computed in the model with

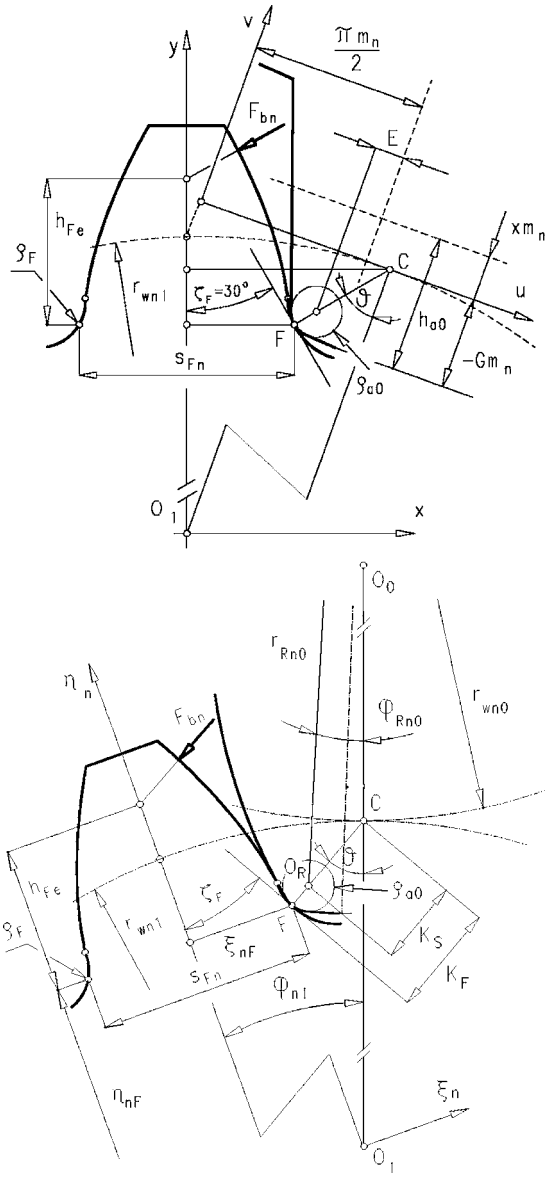

Fig. 13 Determination of parameters of the critical section: s_{Fn}, h_{Fe}, and ρ_F, according to the ISO standard (top) and according to the AGMA standard (bottom)

basic rim thickness $s_R=2.0^*m_n$, the maximum tooth-root stress computed in the model with rim thickness of magnitude i^*s_R, respectively. The basic finite element model used for all further FEM strength computations, i.e., the model with rim thickness defined as $i^*s_R=1.0^*s_R=2.0^*m_n$, is shown in Fig. 2, and the corresponding 2D plane stress finite element model is shown in Fig. 1.

Absolute values of the computed differences $\Delta\sigma_{\text{eff}}(^*1, ^*i)$ are shown in Fig. 8. From the simulations results it follows that the maximum difference in the maximum tooth-root stresses between the investigated models for $i \geq 0.75$, which is equivalent with condition $s_R \geq 1.5^*m_n$, is less than 2% (Fig. 8). That difference reaches appox. 20% at the end of fillet for $i=4.0^*s_R$. The difference of 20% occurs in that case, however, in the areas where the effective stresses are more than three times smaller than the maximum effective tooth-root stress. As far as the maximum tooth-root stresses at the critical section are concerned, the absolute values of the computed differences $\Delta\sigma_{\text{eff}}(^*1, ^*i)$ for $i=0.6^*s_R$ and $i=0.5^*s_R$ reach approx. 8% and 16%, respectively (Fig. 8). From the conducted analysis it follows, that the rim effect takes place for $i<0.75$. Therefore, influence of rim thickness in developed FEM models used for further computations, i.e., models with $i=1.0$, on the maximum tooth-root stress is negligible.

Distributions and magnitudes of effective stress at tooth root in 2D and 3D isoparametric models are almost the same (Figs. 6 and 7). In all models the critical sections were located very close to each other (abscissas of local maxima in Fig. 6). The models built of 3D 20-node isoparametric and eight-node brick finite elements are a more realistic representation of real gears than the 2D finite element models. However, the effective stresses at tooth root computed for the 2D plane stress model differ not more than 5% from the effective tooth-root stresses computed for the 3D models of the whole gear. Moreover, increasing two times and four times the basic thickness of gear rim changes the maximum tooth-root stresses less than 2%.

In all 2D and 3D finite element models generally isoparametric quadrilateral or brick finite elements with very regular rule-based mesh were used. They give more flexibility in precise modeling of the gear shape, at least in the case of rule-based meshes, which is very important in precise modeling of tooth flank and fillet. They also give more flexibility in modeling of strength properties, because they use higher order shape functions than simple tetrahedral elements [16,17]. The triangle and tetrahedral elements were omitted, as their linear shape functions are too primitive to correctly model curvilinear geometry and stresses as compared to the quadrilateral and brick elements, respectively.

From the comparison of results obtained for the various finite element models of gears it follows that application of the precise 2D plane stress finite element models for the analysis of tooth root strength, especially its maximum magnitudes and location of critical section in spur gears is justified. Analysis of tooth root stress of helical gears requires 3D models. However, as it follows from results obtained for the 3D finite element models of the whole gear and three-tooth segment (Figs. 6 and 7), simulations of the three-tooth segment are sufficiently accurate for computations of the local tooth-root stresses at the root of loaded tooth. The detailed results of the 3D finite element simulations of helical gears are given in Sec. 4.

Generally, it is important to mention that both analyzed standards, i.e., ISO and AGMA, clearly indicate the finite element method as one of the most precise methods for computations of tooth strength. Therefore, considering the approach given in the ISO and AGMA standards, and considering the obtained simulations results, it can be concluded that: (1) the developed 2D finite element plane stress models represent tooth-root strength of spur gears with good accuracy, and, thus they will be used in this paper; and (2) in the case of helical gears, the 3D models will be used.

3 Determination of Geometric and Strength Parameters and Factors

3.1 Loads. In both standards tooth-root stresses are calculated for the unit nominal load. The load in the plane of action normal to the tooth flank is converted to the nominal tangential load at the reference diameter F_t (ISO standard) or to the transmitted tangential load at the operating pitch diameter F_{wt} (AGMA standard)—Table 1.

3.2 Critical Section. In both standards it is assumed that maximum stress at tooth root occurs at the critical section, which

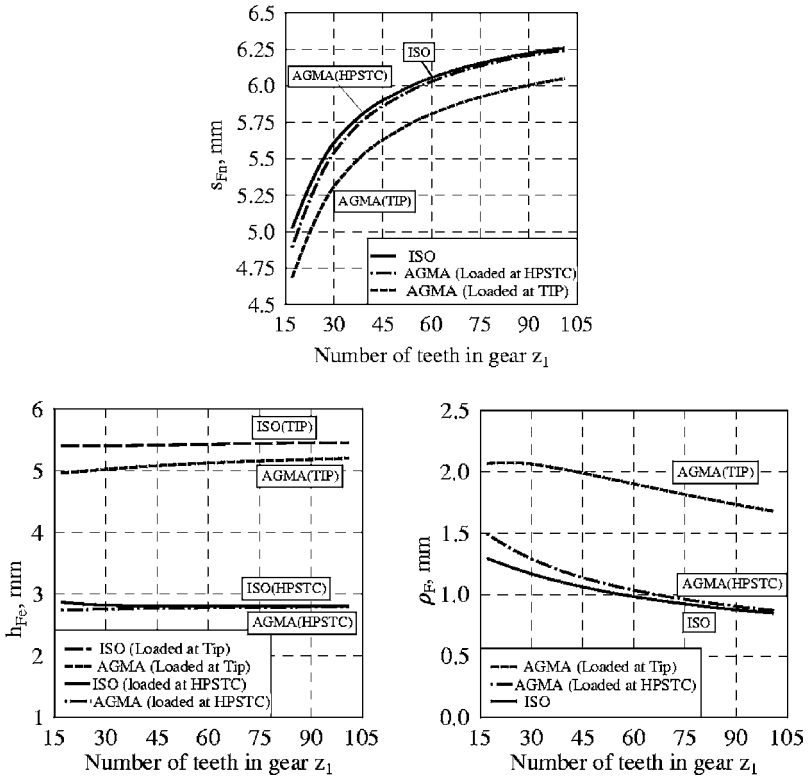

Fig. 14 Influence of the number of gear teeth z_1 on parameters of the critical section: s_{Fn}, h_{Fe}, ρ_F according to the ISO, AGMA for load applied at the tip (Tip), and at the HPSTC; main parameters of the rack (generating tool) and gear are the same as in Fig. 10

is determined in two different ways specific for each standard (Fig. 9 and Table 2).

The magnitudes of the angle ζ_F based on the ISO and AGMA standards, and calculated for different parameter values of the manufactured gears and generating tools as well as for different load cases, are shown in Figs. 10–12.

The angles ζ_F calculated on the basis of the ISO and AGMA standards are compared with the angles representing location of the critical section determined with the use of the finite element method [16,17] in ADINA [42]. For this purpose tooth forms were precisely modeled with fine mesh consisting of eight-node plane stress isoparametric finite elements. Suitable automatic analysis of the results, focused on searching for location of the maximum stresses at tooth root, allowed determination of magnitudes of the angle ζ_F (i.e., slope of the line tangent to the fillet at the point of the computed maximum stress) for a wide range of considered spur gears models.

Figure 10 presents results of computations performed for gearings with different number of teeth z_1 generated with the same rack. According to the AGMA standard the angle ζ_F grows with increasing number of gear teeth z_1 (Fig. 10). In the case when the number of teeth of generated gear z_1 varies in the range $\langle 17, 101\rangle$ and load is applied at the HPSTC the angle ζ_F increases from $\zeta_F=24$ deg to $\zeta_F=29.2$ deg. When the same load is applied at the tooth tip the angle ζ_F increases from $\zeta_F=13.2$ deg to $\zeta_F=16.2$ deg. Also in these cases, according to the ISO standard, the angle ζ_F is constant and equals 30 deg independently from the number of gear teeth.

Figure 11 contains results of computations of the angle ζ_F made for gears generated with gear tools with different number of teeth z_0. Similarly to the case of racks, according to the ISO standard the angle ζ_F is constant and equals 30 deg independently from the number of teeth of the tool and from the location of applied load. According to the AGMA standard, this angle decreases slightly with the growing number z_0 and in the case of load applied at the HPSTC it equals approximately 29 deg which is very close to the value assumed in the ISO standard. On the other hand, in the case of load applied at the tip, the angle ζ_F is almost twice less and equals approximately 16 deg. Results obtained with the use of the finite element method significantly differ from the ones calculated with consideration of both ISO and AGMA standards (see Table 3). In the cases of load applied at the HPSTC the angles ζ_F varied in the range $\langle 44.25\ \text{deg}, 47.25\ \text{deg}\rangle$ and in the cases of load applied at the tip the angles ζ_F varied in the range $\langle 36.0\ \text{deg}, 38.8\ \text{deg}\rangle$. Different magnitudes of the angle ζ_F between tooth center line and tangent to fillet at the critical point F calculated in accordance with the ISO and AGMA standards for different values of the normal module m_n are shown in Fig. 12.

3.3 Parameters of the Critical Section. The following parameters of the critical section (Figs. 9 and 13) are necessary in order to calculate stress at tooth root: tooth-root chord at the critical section s_{Fn}; tooth-root fillet radius of the critical section ρ_F and bending moment arm application at the tooth tip h_{Fe}.

The differences between the ISO and AGMA standards in determination of location of the critical section causes that for the same parameters of gearings and generating tools the parameters of the critical section can significantly differ from each other. This further results in differences in calculated stresses. The selected parameters are calculated in accordance with the ISO and the AGMA standards and are compared in Figs. 14–17.

Figure 14 shows the parameters of the critical section for gearings with various number of teeth z_1 generated with rack and Fig. 15 shows the parameters for gearings generated with gear tools with various number of teeth z_0. In all examples the parameters

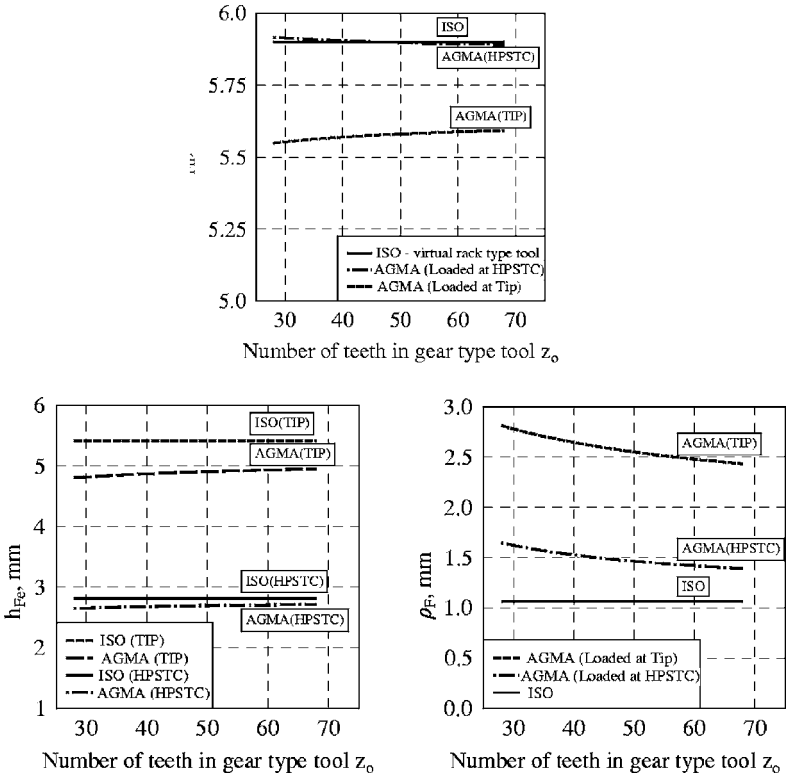

Fig. 15 Influence of the number of teeth z_0 of the gear tool on parameters of the critical section: s_{Fn}, h_{Fe}, ρ_F according to the ISO, AGMA for load applied at the tip (Tip) and at the HPSTC; main parameters of the gear tool (generating tool) and gear are the same as in Fig. 11

were computed for load applied at the highest point of single tooth contact (HPSTC) and for load applied at the tip (Tip).

In the case of gears generated with rack and loaded at the HPSTC, results of calculations of the parameters s_{Fn}, h_{Fe}, ρ_F performed in accordance with the ISO standard are close to the corresponding results obtained on the basis of the AGMA standard (Figs. 14 and 15).

Slightly bigger differences occur between the results for load applied at the tip. In the case of gears generated with gear tools, the differences are more significant, especially, for load applied at the tip. It follows from the fact that according to the ISO standard the calculations are made not for real gear tool used in gear manufacturing but for a virtual rack with the same reference tooth form.

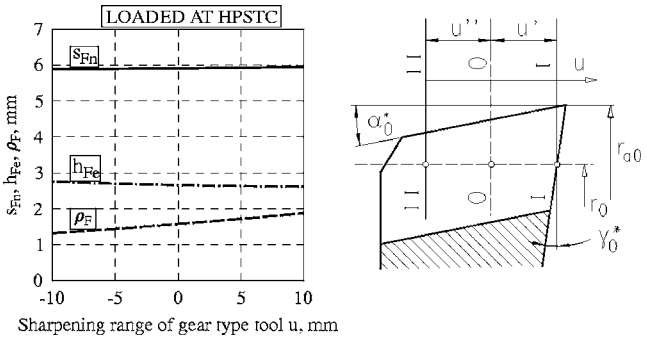

Fig. 16 Influence of the range of sharpening of gear tool (parameter *u*) on parameters of the critical section: s_{Fn}, h_{Fe}, ρ_F according to the AGMA standard for load applied at the HPSTC (left), the range of sharpening of gear tool (right); main parameters of the gear tool (generating tool), and the gear in section 0-0 are the same as in Fig. 11

Therefore, calculations made in accordance with the ISO standard do not consider either influence of the number of teeth of the tool z_0 or a sharpening range of the tool (in the case of gear tool each sharpening of the tool induces changes in parameters of the tool and changes in some parameters of the generated gear—Fig. 16).

Calculations made for gears with different magnitudes of the normal module m_n show that all parameters of the critical section are nearly proportional to the normal module (Fig. 17).

3.4 Coefficients Used in Computational Procedures. In order to calculate nominal tooth-root stresses in accordance with both the ISO and AGMA standards, it is necessary to calculate certain coefficients, which take into account profile of the fillet (parameters of the critical section), complex stress state in tooth root and concentration of stresses caused by a geometric notch (fillet at tooth root). Methods of calculation of these coefficients are given in Table 4.

In both standards, calculations for the helical gearings are performed the same way as in the case of spur straight tooth gearings with the virtual number of teeth z_n. An influence of the helical tooth trace on tooth-root strength is additionally taken into account by related coefficients. In the ISO standard it is a helix angle factor Y_β (Table 4). In the AGMA standard the formula for the bending strength geometry factor Y_J considers the load sharing ratio m_N (in the case of spur gears m_N=1.0) and the formula for the tooth form factor Y considers β and β_w, i.e., helix angle at the reference cylinder and helix angle at the operating pitch cylinder, respectively (Table 4).

3.5 Load Factors. The stresses at tooth root result from real loads transmitted in gear transmission and not from nominal ones. Therefore, both ISO and AGMA standards consider the corresponding load factors (Table 5). These factors take into account increase of stresses due to errors arising in gear transmission

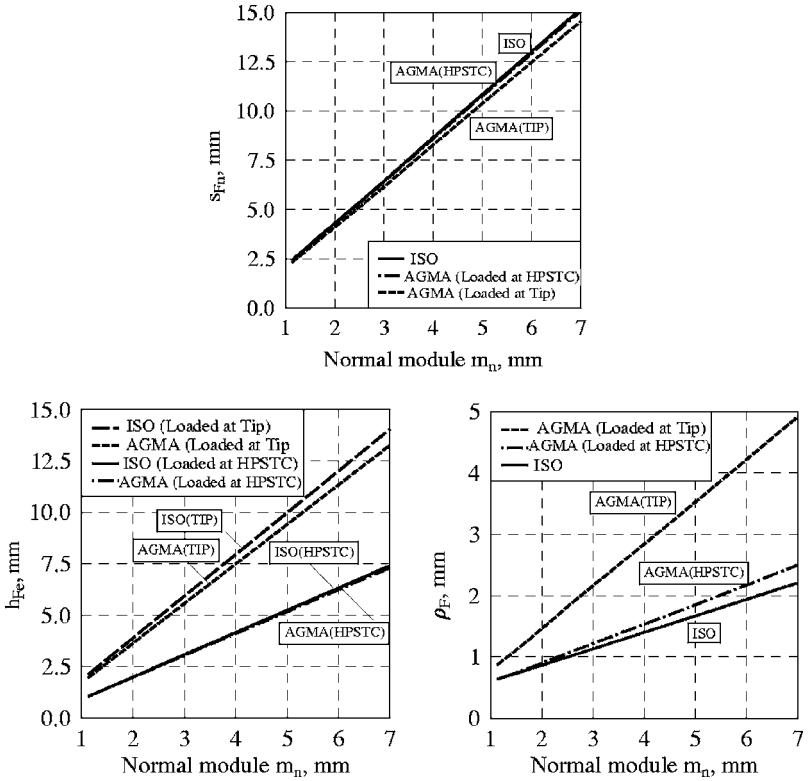

Fig. 17 Influence of the normal module m_n on parameters of the critical section: s_{Fn}, h_{Fe}, ρ_F according to the ISO and AGMA standards for load applied at the tip (Tip), and at the HPSTC; main parameters of the rack (generating tool) and gear are the same as in Fig. 12

manufacturing, due to internal and external dynamic loads and non-uniform distribution of loads in gear transmission. The standards contain suitable formulas or tables based on which one can determine values of the load factors.

3.6 Stress at Tooth Root. Stress at tooth root is considered in both ISO and AGMA standards as a representative parameter in the evaluation of tooth-root strength of gear. First-nominal tooth-root stress σ_{FO} is calculated for the nominal load and for the assumed form of the fillet and parameters of the critical section. Then, the stress is recalculated with the use of the load factors (Table 5) to get local tooth-root stress σ_F (Table 6).

The objective of this work is to compare influence of tooth geometry (resulting from applied method of gear generation and from parameters of the tools) on the tooth-root strength, according to both the ISO and AGMA standards. Therefore, in all computations the load factors (Table 5) were not taken into account, as they do not introduce any new information as far as the analysis of influence of tooth geometry on tooth-root strength is considered.

4 Analysis of Tooth-Root Stresses According to the ISO and AGMA Standards and FEM

Stresses calculated for various models of gears in accordance with the ISO and AGMA standards as well as based on the FEM models developed in the ADINA [42] environment, are compared in Figs. 18–25. Results of computations made for gears with different number of teeth z_1 generated with racks are shown in Fig. 18. Similarly, as in the case of parameters calculations of the critical section given in Sec. 3.3, computations of tooth-root stress were made for two load cases: for load applied at the highest point of single tooth contact and for load applied at the tip, respectively.

Figure 19 presents stresses calculated for gears manufactured with gear tools for various number of teeth z_0, Figure 20 shows stresses calculated for gear manufactured with one exemplary gear tool, but with different magnitudes of parameter u related to the geometric effect of tool sharpening. In the ISO standard any real gear tool is replaced with a related virtual rack. Therefore, tooth-root stresses calculated in accordance with this standard are constant, i.e., they do not depend on the parameters z_0 and u.

Influence of some other important geometric parameters of gears, like normal pressure angle α_n, addendum modification coefficient x_1, helix angle at the reference cylinder β_1, and normal module m_n on magnitude of tooth-root stress are given in Figs. 21–25, respectively.

The models of helical gears were built of 3D 20-node isoparametric and eight-node brick finite elements. They represented three teeth segments of gears with load applied to the central tooth in the most unfavorable case (assuming no misalignments in gear axes) of load distributed along the diagonal line of contact passing through the tip corner of tooth flank. The boundary conditions reflected the ones shown in Fig. 1, and were applied on corresponding boundary surfaces of the 3D models of gear segments. Distributions of the effective stresses along tooth line passing through critical sections in various FEM models of helical gears with different helix angles β and along fillet in various transversal sections of helical gear with helix angle β=17 deg are shown in Fig. 24.

In all performed computations, tooth-root stresses obtained according to the ISO standard were greater than the tooth-root stress calculated according to the AGMA standard. The difference was bigger in the case of load applied at the tip than in the case of load applied at the HPSTC. Stresses computed with the use of the finite element method were in between, i.e., were greater than stresses according to the AGMA and smaller than stresses according to the ISO standard.

Comparison of locations of the critical section and the angle

Table 4 Computational coefficients

ISO	AGMA
Tooth form factor Y_F: This factor considers influence of shape of tooth at the tooth-root stress. This shape is defined in computational procedure by the parameters of the critical section $$Y_F=\frac{6(h_{Fe}/m_n)\cos\alpha_{Fen}}{(s_{Fn}/m_n)^2\cos\alpha_n}$$ where: α_{Fen}-load angle; α_n-normal pressure angle at the pitch cylinder.	***Tooth form factor Y***: This factor considers influence of shape of tooth at the tooth-root stress. This shape is defined in computational procedure by the parameters of the critical section $$Y=\frac{\cos\beta_w\cos\beta}{\frac{\cos\alpha_{Fen}}{\cos\alpha_{wn}}\left[\frac{6h_{Fe}}{s_{Fn}^2C_h}-\frac{tg\alpha_{Fen}}{s_{Fn}}\right]}$$ where: α_{Fen}-load angle; α_{wn}-operating normal pressure angle; β-helix angle at the reference cylinder; β_w-operating helix angle; C_h-helix factor.
Helix angle factor Y_β: This factor considers difference in stresses at tooth root between helical gear and virtual spur gear with straight teeth used for calculations $$Y_\beta=1-\varepsilon_\beta\frac{\beta}{120}$$	***Helix factor C_h***: The helix factor C_h is calculated in the following way:-for spur gears $C_h=1.0$ -for conventional helical gears $$C_h=\frac{1}{1-\left[\frac{\omega}{100}\left(1-\frac{\omega}{100}\right)\right]^{0.5}}$$ where: $\omega=arctg(tg\beta\sin\alpha_n)$
Stress correction factor Y_S: This factor considers complex stress state at tooth root and stress concentration caused by the fillet (geometric notch) $$Y_S=(1.2+0.13L)q_s^a$$ where: $L=s_{Fn}/h_{Fe}$; $q_s=s_{Fn}/(2\rho_F)$; $a=[1.21+2.3/L]^{-1}$	***Stress correction factor K_f***: This factor considers complex stress state at tooth root and stress concentration caused by the fillet (geometric notch) $$K_f=H+\left(\frac{s_{Fn}}{\rho_F}\right)^L\left(\frac{s_{Fn}}{h_{Fe}}\right)^M$$ where: $H=0.331-0.436\alpha_n$; $L=0.324-0.492\alpha_n$; $M=0.261+0.54\alpha_n$ ***Bending strength geometry factor Y_J***: This factor is calculated from the equation $$Y_J=\frac{YC_\psi}{K_fm_N}$$ where: C_ψ-helical overlap factor (for spur and conventional helical transmissions $C_\psi=1.0$); m_N- load sharing ratio (for spur gears $m_N=1.0$; for helical gears $m_N=b/L_{\min}$); b-effective face width; $L_{\min}$-minimum length of contact lines.

Table 5 Load factors

ISO	AGMA
K_A - application factor: considers variations of external loads acting on gear transmission in relation to the nominal load (Table 1); K_v - dynamic factor: considers internal dynamic loads caused by vibrations of pinion and gear; $K_{F\beta}$ - face load factor (root stress): considers possible non-uniform distribution of load along contact line; $K_{F\alpha}$-transverse load factor (root stress): considers distribution of load between the pairs of teeth in contact, including non-uniform distribution of load along path of contact [27].	K_o - overload factor; K_v - dynamic factor; K_H - load distribution factor; K_S - size factor: considers influence of size of gearing on tooth-root stress; K_B - rim thickness factor [33].

Table 6 Stress at tooth root

ISO	AGMA
Nominal tooth-root stress σ_{F0} [27]: $$\sigma_{F0}=\frac{F_t}{bm_n}Y_FY_SY_\beta$$ Local tooth-root stress σ_F: $\sigma_F=\sigma_{F0}K_AK_vK_{F\alpha}K_{F\beta}$	Local tooth-root stress σ_F [33,34] $$\sigma_F=F_tK_oK_vK_S\frac{1}{bm_t}\frac{K_HK_B}{Y_J}$$ where: m_t-transverse module

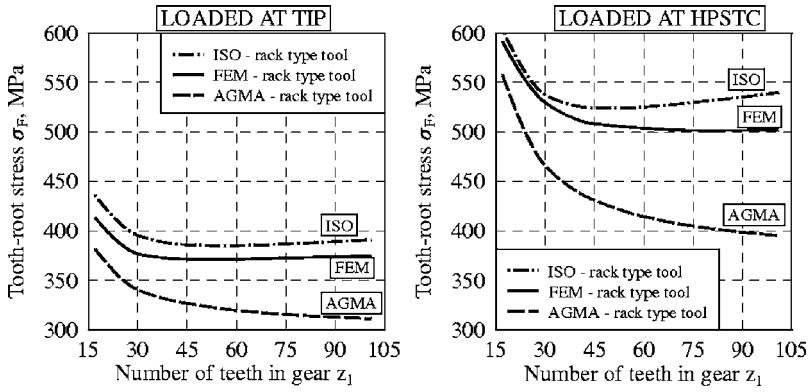

Fig. 18 Influence of the number of gear teeth z_1 on tooth-root stress σ_F according to the ISO standard, AGMA standard, and FEM: for load applied at the tip F_{bn}/b=250 N/mm (left) and for load applied at the HPSTC F_{bn}/b =500 N/mm (right); main parameters of the rack (generating tool) and gear are the same as in Fig. 10

between tangent to fillet and tooth center line computed according to the ISO and AGMA standards as well as according to the precise finite element analysis is shown in Fig. 26.

Different locations of critical section at tooth root is caused by the fact that ISO and AGMA standards use different methods to determine critical section. This leads to different magnitudes of critical section parameters, such as: h_{Fe}, s_{Fn}, ρ_F,. Additionally, both standards determine these parameters by using different formulas. Varying locations of critical section are the main reason of differences in tooth-root stresses, which can be seen in Figs. 18–23.

In the case of gears manufactured with racks, stresses computed with the use of the finite element method were closer to the results of the ISO standard. In the cases of gears manufactured with gear tools, stresses computed with the use of the finite element method were closer to the results of the AGMA standard. Absolute differences in stresses calculated in accordance with the ISO and AGMA standards diminish with growing normal module m_n (Fig. 25).

5 Summary and Conclusions

This paper conducts a comprehensive analysis of the geometrical parameters and their impact on gear performance as described by the ISO [27] and AGMA [29–37] standards with FEM computations conducted by the authors. Furthermore, the presented analysis leads to suggestions and recommendations which can be used in future preparation of gear standards. The presented comparative analysis is important for modern design and manufacturing of gears conducted globally at various locations. Current trends in engineering globalization necessitate revisiting various normalized standards to determine their common fundamentals and best approaches needed to develop "best practices" in automotive, aerospace and other industries [1,2,48,49]. This can lead to both reduction in redundancies and also cost containment related to needed adjustments between manufacturers for missing part interchangeability and performance due to incompatibility of different standards. Also, currently many manufacturers are faced with the necessity of obtaining certificates of their products in Europe, USA, or in Asia.

Therefore, in this paper methods of evaluation of tooth-root strength according to the ISO and AGMA standards are compared by matching: (i) formulas used in both standards; (ii) estimation of critical section location (determined by the angle ζ_F between tooth centerline and tangent to fillet at the critical point F), and (iii) parameters of the critical section and tooth-root stresses. Calculations were performed for gears generated with racks and gear tools for various combinations of main parameters of gear geometry and tools used for manufacturing as well as for different locations of load application. Stresses determined in accordance with the ISO and AGMA standards are compared with results of

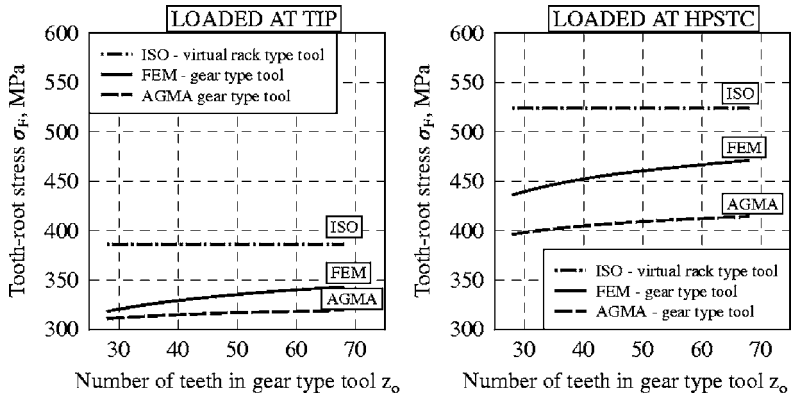

Fig. 19 Influence of the number of teeth z_0 of the gear tool on tooth-root stress σ_F according to the ISO standard, AGMA standard, and FEM: for load applied at the tip (left) and for load applied at the HPSTC (right); main parameters of the gear tool (generating tool) and gear are the same as in Fig. 11; magnitude of load is the same as in Fig. 18

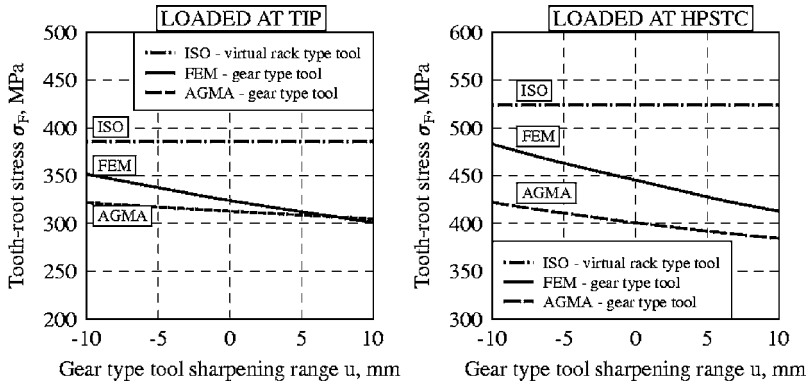

Fig. 20 Influence of the range of sharpening of gear tool (parameter u) on tooth-root stress σ_F according to the ISO, AGMA, and FEM: for load applied at the tip (left) and for load applied at the HPSTC (right); main parameters of the gear tool (generating tool) and the gear in section 0-0 are the same as in Fig. 11; magnitude of load is the same as in Fig. 18

related finite element analysis of the gears. Conclusions following from the performed analysis can be grouped in these categories.

1. **Strength of helical gears**. In both standards tooth-root strength analysis is performed for virtual straight tooth spur gearing with virtual number of teeth z_n.

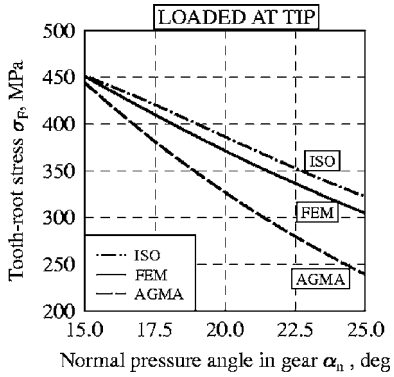

Fig. 21 Influence of the normal pressure angle α_n on tooth-root stress σ_F according to the ISO, AGMA, and FEM: for load applied at the tip; main parameters of the gear: m_n=2.75, z_1 =45, s_1=4.265, β_1=0 deg; main parameters of the rack (generating tool): s_0=4.320, ρ_{fP}=0.18m_n; magnitude of load is the same as in Fig. 18

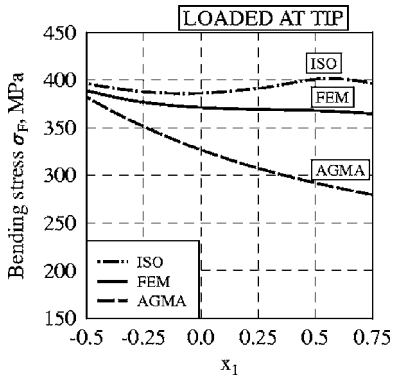

Fig. 22 Influence of the addendum modification coefficient x_1 on tooth-root stress σ_F according to the ISO, AGMA, and FEM: for load applied at the tip; main parameters of the gear: m_n =2.75, α_n=20 deg, β_1=0 deg; main parameter of the rack (generating tool): ρ_{fP}=0.18m_n; magnitude of load is the same as in Fig. 18

2. **Strength of gears manufactured with racks**. In the ISO, standard calculations are performed for rack with assumed standard basic rack tooth profile. In the AGMA, standard calculations are made for virtual gear tool with the same standard basic rack tooth profile and very large number of teeth (z_0=10.000).
3. **Strength of gears manufactured with gear tools**. In the ISO standard real gear tool is replaced with virtual rack with the same standard basic rack tooth profile. This significantly simplifies calculations though it may lead to incorrect results in parameters of the critical section and in tooth-root stress (tooth profiles generated with gear tools and racks can significantly differ from each other). In the AGMA standard calculations are done for real gear tool.
4. **Location of the critical section**. Methods of determination of the critical section are different in the ISO standard and in the AGMA standard. This leads to magnitudes of the angle ζ_F between tooth centerline and tangent to fillet at the critical point F and the parameters of the critical section: s_{Fn}, h_{Fe}, and ρ_F. In the case of load applied at the HPSTC the differences are relatively small. However, in the case of load applied at the tip the differences are meaningful.
5. **Tooth-root stress**. In both standards, evaluation of tooth-root strength is performed based on maximum stress at tooth root on the stretched side of the tooth. It is assumed that the

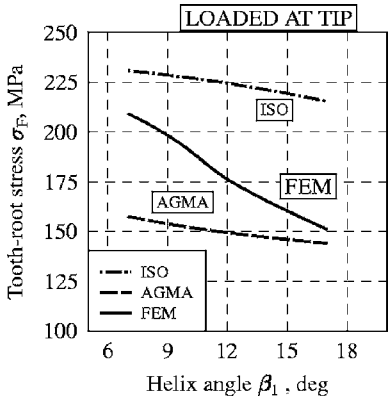

Fig. 23 Influence of the helix angle β_1 on tooth-root stress σ_F according to the ISO, AGMA, and FEM for load applied at the tip; main parameters of the gear: m_n=5.0, z_1=24, α_n=20 deg, magnitude of distributed load passing through the tip corner of helical tooth flank F_{bn}/b=274 N/mm

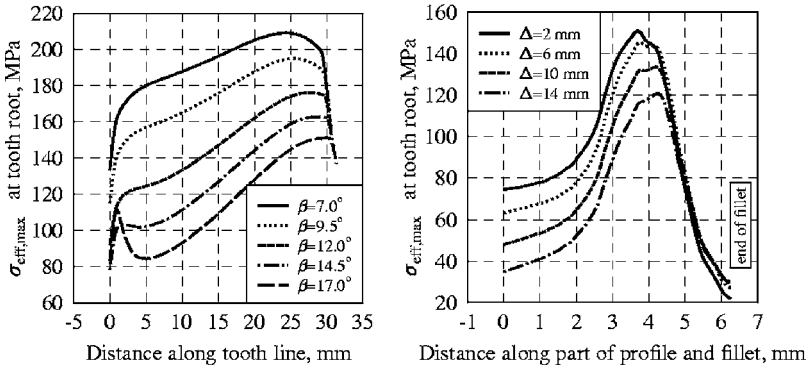

Fig. 24 Distribution of the effective stresses along tooth line passing through critical sections in various finite element models of helical gears with different helix angles β (left) and along fillet in various transversal sections of helical gear with helix angle β=17 deg (right); main parameters of the gear: m_n=5.0, z_1=24; magnitude of distributed load passing through the tip corner of helical tooth flank F_{bn}/b=274 N/mm; parameter Δ used for determination of location of transversal sections of tooth is illustrated in Fig. 7 left

maximum stress occurs in the critical section of the tooth. Differences in tooth-root stresses calculated according to the ISO and AGMA standards (Figs. 18–25) are caused by application of different formulas for tooth form factor and stress correction factor (Table 4). Those coefficients are computed in both standards using the same parameters of critical section. However, in the formula defining tooth form factor, Y in AGMA, there exists an additional component $\mathrm{tg}\alpha_{Fen}/s_{\mathrm{Fn}}$, which does not exist in the corresponding formula for tooth form factor Y_F in the ISO standard. Formulas for stress correction factor (Y_S according to ISO and K_f according to AGMA) differ, first of all, in applied exponents (Table 4). As a result of that, even in the case when computations are made for load applied at the HPSTC (for which case differences in both location and parameters of critical section determined according to ISO and AGMA standards are insignificant - Figs. 10–12, 14, 15, and 17), computed tooth-root stresses differ from each other. Those differences in tooth-root stresses calculations according to the ISO and AGMA standards are bigger in the case when computations are conducted for load applied to tooth tip than to HPSTC. This is caused by the fact that considered ISO and AGMA standards differently determine both location and parameters of critical section (Fig. 9). In all considered cases tooth-root stresses calculated in accordance with the ISO were bigger than corresponding results according to the AGMA. At the same time, the difference in tooth-root stress was much bigger in the case of load applied at the tip than in the case of load applied at the HPSTC. Results of finite element computations were bigger than AGMA and smaller than ISO results. In the case of gears generated with racks stresses computed with finite elements were closer to the ISO results and in the case of gears generated with gear tools they were closer to the AGMA results.

6. **Influence of geometric parameters of gearing on tooth-root strength**. Both standards differ in evaluation of an influence of the helix angle β_1, pressure angle α_1, and addendum modification coefficient x_1 on tooth-root strength (Figs. 20–25).

Detailed conclusions following comparison of related formulas and results of calculations are given in corresponding sections of this paper.

Appendix

In order to enable comparison of corresponding relations between considered parameters used in the ISO and AGMA standards, one of them should be presented and analyzed in relation to the other. Nomenclature used in this paper follows the ISO standard [27]. Original AGMA nomenclature is given in Table 7. The

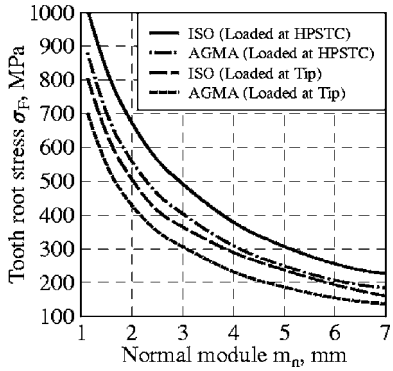

Fig. 25 Influence of the normal module m_n on tooth-root stress σ_F according to the ISO and AGMA for load applied at the tip (Tip) and at the HPSTC; main parameters of the generating rack and gear are the same as in Fig. 12; magnitude of load is the same as in Fig. 18

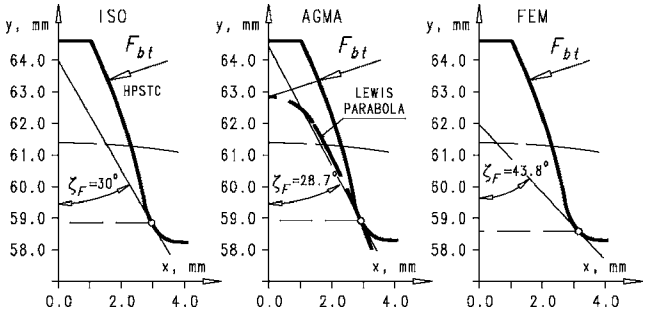

Fig. 26 Comparison of locations of the critical section and the angle between tangent to fillet and tooth centerline computed according to the ISO (left) and AGMA (middle) standards as well as according to the precise finite element analysis (right) of the gears with the same tooth profiles; magnitude of load is the same as in Fig. 18

Table 7 List of symbols

ISO	AGMA	Name of parameter	Unit
α_{Fen}	ϕ_{nL}	Load angle	deg, rd
α_n	α_n	Standard normal pressure angle	deg, rd
α_{wn}	α_{wn}	Operating normal pressure angle	deg, rd
β	β	Helix angle at the reference cylinder	deg, rd
β_w	β_w	Operating helix angle	deg, rd
ε_α	m_p	Transverse contact ratio	deg, rd
ε_β	m_F	Overlap ratio, axial contact ratio	⋯
φ_{Rn0}	μ_{n0}	Auxiliary angle locating the center of tool tip radius	deg, rd
ρ_F	ρ'_F	Radius of curvature of fillet curve (at the critical point F)	mm
ρ_{fP}, ρ_{a0}	ρ_{a0}	Root fillet radius of the basic rack, tool tip radius	mm
σ_F	σ_F	Tooth-root stress, bending stress number	MPa
σ_{F0}	⋯	Nominal tooth-root stress	MPa
ζ_F	β_n	Angle between tangent to fillet at the critical point F and tooth centerline	deg, rd
ϑ	⋯	Auxiliary angle used for calculation of parameters of the critical section (Fig. 13)	deg, rd
	ζ_{nF}, η_{nF}	Abscissa and ordinate of critical point F	
b	b	Effective face width (ISO), net face width of narrowed member (AGMA)	mm
d_1, d_2	d_1, d_2	Standard pitch diameter, pinion (1) and gear (2)	mm
r_1, r_2	r_1, r_2	Standard pitch radii, pinion (1) and gear (2)	
d_{bn1} d_{bn0}	d_{nb1}, d_{bn0}	Virtual base diameter (radius) of pinion (1),	mm
r_{bn1}, r_{bn0}	r_{nb1}, r_{nb0}	Virtual base diameter (radius) of gear type tool (0)	
d_{en} (r_{en})	d_{nL} (r_{nL})	Virtual load diameter (radius)	mm
d_{w1}, d_{w2}	d_{w1}, d_{w2}	Operating diameter, pinion (1) and gear (2)	mm
r_{w1}, d_{w2}	r_{w1}, d_{w2}	Operating radius, pinion (1) and gear (2)	
E	⋯	Distance from the center of rounded tip of tool to the axis of tooth	mm
F_{bn}	⋯	Transmitted load in the plane of action (normal to the tooth flank)	N
F_t	F_t	Transmitted tangential load at the pitch diameter (ISO), transmitted tangential load at the operating pitch diameter (AGMA)	N
h_{Fe}	h_F	Bending moment arm	mm
h_{fP}, h_{a0}	h_{a0}	Tooth dedendum of the virtual basic rack, nominal tool addendum	mm
K_A	⋯	Application factor for bending strength	⋯
$K_{F\alpha}$	$K_{F\alpha}$	Transverse load distribution factor (root stress)	⋯
$K_{F\beta}$	$K_{F\beta}$	Face load distribution factor (root stress)	⋯
K_v	K_v	Dynamic factor for bending strength	⋯
m_n	m_n	Normal module	mm
m_t	m_t	Transverse module	mm
r_{Rn0}	r_{Sno}	Radius to center of tool tip radius	mm
r_{wn1}, r_{wn0}	r''_n, r''_{n0}	Generating pitch radius of virtual spur gear (1), virtual tool (0)	mm
s_1, s_0	s_n, s_{n0}	Reference normal circular tooth thickness of gear (1), of tool (0)	mm
s_{Fn}	s_F	Tooth thickness at critical section	mm
s_{pr}	δ_{a0}	Amount of effective protuberance	mm
T_1, T_2	T_1, T_2	Torque on the pinion (1), gear (2)	Nm
Y_β	C_h	Helix angle factor	⋯
Y_F	Y	Tooth form factor	⋯
Y_S	K_f	Stress correction factor	⋯
z_0	⋯	Number of tooth of gear-type tool	
z_1	z_1	Number of tooth of pinion	⋯
⋯	K_B	Rim thickness factor	⋯
	K_F	Distance from pitch point C to point F (Fig. 13)	
⋯	K_H	Load distribution factor	⋯
⋯	K_o	Overload factor	⋯
	K_S	Distance from pitch point C to point O_R (Fig. 13)	
⋯	K_s	Size factor	⋯
	$L_{\min}$	Minimum length of contact lines	mm
	m_N	Load sharing ratio	⋯
	Y_J	Bending strength geometry factor	⋯

Table 7 contains symbols, descriptions, and units used for corresponding parameters in the ISO [27] and AGMA [29,33] standards considered in this paper.

References

[1] Ceglarek, D., Huang, W., Zhou, S., Ding, Y., Kumar, R., and Zhou, Y., 2004, "Time-Based Competition in Manufacturing: Stream-of-Variation Analysis (SOVA) Methodology—Review," Int. J. of Flexible Manuf. Syst., **16**(1), pp. 11–44.

[2] Anderson, N. et al., 2004, "Gear Industry Vision. A Vision of Gear Industry in 2025," Technical Report developed at the Gear Industry Vision Workshop, March 10, 2004, Detroit. The report was prepared by Energetics, Inc., and sponsored by U.S. Army, AGMA Foundation, ASME CRTD, Ben Franklin Technology Center, Boeing, Gleason Foundation, GM, and John Deere.

[3] Dudley, D. W., 2002, *Handbook of Practical Gear Design*, CRC, Boca Raton, FL.

[4] Townsend, D. P., 1992, *Dudley's Gear Handbook*, McGraw–Hill, New York.

[5] Smith, J. D., 1999, *Gear Noise and Vibration*, Dekker, New York.

[6] Badgley, R. H., and Hartman, R. H., 1974, "Gearbox Noise Reduction: Prediction and Measurement of Mesh-Frequency Vibrations Within an Operating

Helicopter Rotor-Drive Gearbox," Trans. ASME J. Eng. Ind., **96**(2), pp. 567–577.
[7] Cavdar, K., Karpat, F., and Babalik, F. C., 2005, "Computer Aided Analysis of Bending Strength of Involute Spur Gears with Asymmetric Profile," ASME J. Mech. Des., **127**(3), pp. 477–484.
[8] Wang, M.-J., 2003, "A New Photoelastic Investigation of the Dynamic Bending Stress of Spur Gears," ASME J. Mech. Des., **125**(2), pp. 365–372.
[9] Velex, P., and Baud, S., 2002, "Static and Dynamic Tooth Loading in Spur and Helical Geared Systems—Experiments and Model Validation," ASME J. Mech. Des., **124**(2), pp. 334–346.
[10] Winter, H., and Hirt, M., 1974, "Zahnfußtragfähigkeit auf der Grundlage der Wirklichen Spannungen. Spannungskorrekturfaktor, Kerbempfindlichkeitszahl und Relativer Kerbfaktor in ISO-Ansatz," VDI-Z, **116**(2), pp. 119–126.
[11] Linke, H., and Sporbert, K., 1985, "Einfluß des Schleifabsatzes auf die Spannungs-Konzentration bei Verzahnungen," Maschinenbautechnik, **34**(4), pp. 251–257.
[12] Jaśkiewicz, Z., and Wąsiewski, A., 1992, *Spur Gear Transmissions. Geometry, Strength, Accuracy of Manufacturing* (in Polish), **1**, Transport and Communication, Warsaw.
[13] Jaśkiewicz, Z., and Wąsiewski, A., 1995, *Spur Gear Transmissions. Design* (in Polish), **2**, Transport and Communication, Warsaw.
[14] Litvin, F. L., Egelja, A., Tan, J., and Heath, G., 1998, "Computerized Design, Generation and Simulation of Meshing of Orthogonal Offset Face-Gear Drive With a Spur Involute Pinion With Localized Bearing Contact," Mech. Mach. Theory, **33**(1/2), pp. 87–102.
[15] Pedrero, J. I., Rueda, A., and Fuentes, A., 1999, "Determination of the ISO Tooth Form Factor for Involute Spur and Helical Gears," Mech. Mach. Theory, **34**(1), pp. 89–103.
[16] Bathe, K. J., 1996, *Finite Element Procedures*, Prentice–Hall, Englewood Cliffs, NJ.
[17] Kleiber, M., ed., 1998, *Handbook of Computational Solid Mechanics*, Springer, Berlin.
[18] Weck, M., 1992, *Moderne Leistungsgetriebe. Verzahnungsauslegung und Betriebsverhalten*, Springer-Verlag, Berlin.
[19] Guingand, M., de Vaujany, J. P., and Icard, Y., 2004, "Fast Three-Dimensional Quasi-Static Analysis of Helical Gears Using the Finite Prism Method," ASME J. Mech. Des., **126**(6), pp. 1082–1088.
[20] Sainsot, P., and Velex, P., 2004, "Contribution of Gear Body to Tooth Deflections—A New Bidimensional Analytical Formula," ASME J. Mech. Des., **126**(4), pp. 748–752.
[21] Litvin, F. L., Fuentes, A., Zani, C., Pontiggia, M., and Handschuh, R. F., 2002, "Face-Gear Drive With Spur Involute Pinion: Geometry, Generation by a Worm, Stress Analysis," Comput. Methods Appl. Mech. Eng., **191**(25–26), pp. 2785–2813.
[22] Litvin, F. L., Chen, J. S., Lu, J., Handschuh, R. F., 1996, "Application of Finite Element Analysis for Determination of Load Share, Real Contact Ratio, Precision of Motion, and Stress Analysis," ASME J. Mech. Des., **118**(4), pp. 561–567.
[23] Lewicki, D. G., Handschuh, R. F., Spievak, L. E., Wawrzynek, P. A., and Ingraffea, A. R., 2001, "Consideration of Moving Tooth Load in Gear Crack Propagation Predictions," ASME J. Mech. Des., **123**(1), pp. 118–124.
[24] Handschuh, R. F., and Bibel, G. D., 1999, "Experimental and Analytical Study of Aerospace Spiral Bevel Gear Tooth Fillet Stresses," ASME J. Mech. Des., **121**(4), pp. 565–572.
[25] Barkah, D., Shafiq, B., and Dooner, D., 2002, "3D Mesh Generation for Static Stress Determination in Spiral Noncircular Gears Used for Torque Balancing," ASME J. Mech. Des., **124**(2), pp. 313–319.
[26] Liu, L., and Pines, D. J., 2002, "The Influence of Gear Design Parameters on Gear Tooth Damage Detection Sensitivity," ASME J. Mech. Des., **124**(4), pp. 794–804.
[27] ISO 6336 Standard, Calculation of Load Capacity of Spur and Helical Gears.
[28] DIN 3990, Tragfähigkeitsberechnung von Stirnrädern, Dezember 1987.
[29] AGMA 908-B89, April 1989, Geometry Factors for Determining the Pitting Resistance and Bending Strength of Spur, Helical and Herringbone Gear Teeth.
[30] AGMA 918-A93. AGMA Information Sheet, January 1993, A Summary of Numerical Examples Demonstrating the Procedures for Calculating Geometry Factors for Spur and Helical Gears.
[31] ANSI/AGMA 6002-B93, February 1993, Design Guide for Vehicle Spur and Helical Gears.
[32] ANSI/AGMA 2001-C95, January 1995, Fundamental Rating Factors and Calculation Methods for Involute Spur and Helical Gear Teeth.
[33] ANSI/AGMA 2101-C95, January 1995, Metric Edition of ANSI/AGMA 2001-C95. Fundamental Rating Factors and Calculation Methods for Involute Spur and Helical Gear Teeth.
[34] ANSI/AGMA 6110-F97, September 1997, Standard for Spur, Helical, Herringbone and Bevel Enclosed Drives. Annex C, Illustrative examples.
[35] AGMA Information Sheet 913-A98, Method for Specifying the Geometry of Spur and Helical Gears.
[36] Hösel, T., 1988, "Einfluß der Zahnform auf die Flanken—und Zahnfuβtragfähigkeit nach DIN 3990 und AGMA 218.01—Grenzen für Optimierungsrechnungen," Antriebstechnik, **27**(9), pp. 65–68.
[37] Hösel, T., 1989, "Vergleich der Tragfähigkeitsberechnung für Stirnräder nach ANSI/AGMA—ISO/DIN—und RGW-Normen," Antriebstechnik, **28**(11), pp. 77–84.
[38] Niemann, G., and Winter, H., 1985, *Maschinenelemente, Band II*, Springer-Verlag, Berlin.
[39] Lewicki, D. G., and Ballarini, R., 1997, "Gear Crack Propagation Investigations," Gear Technol., **14**(6), pp. 18–24.
[40] Kawalec, A., and Wiktor, J., 1999, "Analytical and Numerical Method of Determination of Spur Gear Tooth Profile Machined by Gear Tools," Adv. Technol. Mach. Equipment, **23**(2), pp. 5–28.
[41] Math, V. B., and Chand, S., 2004, "An Approach to the Determination of Spur Gear Tooth Root Fillet," ASME J. Mech. Des., **126**(2), pp. 336–340.
[42] *ADINA Theory and Modeling Guide*, ADINA R & D, Inc., Watertown, MA, 2000.
[43] Kawalec, A., 1997, "Modelling of Tooth Flanks Based on Distorted Measurements," Adv. Technol. Mach. Mech. Equipment, **21**(3), pp. 5–28.
[44] Kawalec, A., and Wiktor, J., 2001, "Analysis of Strength of Tooth Root With Notch After Finishing of Involute Gears," Arch. Mech. Eng., **48**(3), pp. 217–248.
[45] Timoshenko, S. P., and Goodyear, J. N., 1970, *Theory of Elasticity*, McGraw–Hill, New York.
[46] Kramberger, J., Šraml, M., Potrč, I., and Flašker, J., 2004, "Numerical Calculation of Bending Fatigue Life of Thin-Rim Spur Gears," Eng. Fract. Mech., **71**(4–6), pp. 647–656.
[47] Li, S., 2002, "Gear Contact Model and Loaded Tooth Contact Analysis of a Three-Dimensional Thin-Rimmed Gear," ASME J. Mech. Des., **124**(3), pp. 511–517.
[48] Ceglarek, DS., Shi, J., and Wu, S. M., 1994, "A Knowledge-based Diagnosis Approach for the Launch of the Auto-body Assembly Process," ASME J. Eng. Ind., **116**(4), pp. 491–499.
[49] Rybak, J., Kawalec, A., and Wiktor, J., 1999, "Analysis in Involute Cylindrical Gear Transmissions with Modified Tooth Trace," Proceedings of the 4th World Congress on Gearing and Power Transmissions, Paris, M.C.I., 1, pp. 169–181.